

# Peptide–Antibody Fusions Engineered by Phage Display Exhibit an Ultrapotent and Broad Neutralization of SARS-CoV-2 Variants

Jonathan M. Labriola,<sup>○</sup> Shane Miersch,<sup>○</sup> Gang Chen, Chao Chen, Alevtina Pavlenko, Reza Saberianfar, Francesca Caccuri, Alberto Zani, Nitin Sharma, Annie Feng, Daisy W. Leung, Arnaldo Caruso, Giuseppe Novelli, Gaya K. Amarasinghe, and Sachdev S. Sidhu\*



Cite This: <https://doi.org/10.1021/acscchembio.2c00411>



Read Online

ACCESS |



Metrics & More

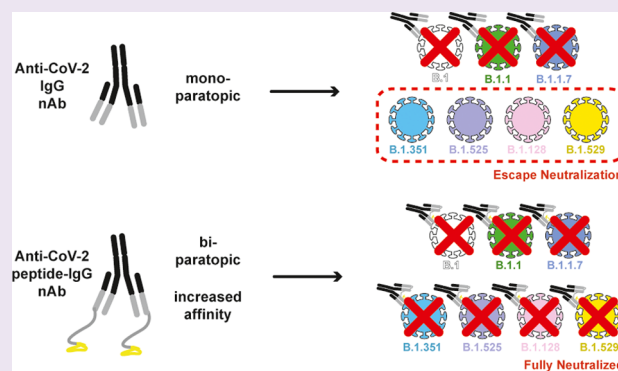


Article Recommendations



Supporting Information

**ABSTRACT:** The spread of COVID-19 has been exacerbated by the emergence of variants of concern (VoC). Many VoC contain mutations in the spike protein (S-protein) and are implicated in infection and response to therapeutics. Bivalent neutralizing antibodies (nAbs) targeting the S-protein receptor-binding domain (RBD) are promising therapeutics for COVID-19, but they are limited by low potency and vulnerability to RBD mutations in VoC. To address these issues, we used naïve phage-displayed peptide libraries to isolate and optimize 16-residue peptides that bind to the RBD or the N-terminal domain (NTD) of the S-protein. We fused these peptides to the N-terminus of a moderate-affinity nAb to generate tetravalent peptide–IgG fusions, and we showed that both classes of peptides were able to improve affinities for the S-protein trimer by >100-fold (apparent  $K_D < 1$  pM). Critically, cell-based infection assays with a panel of six SARS-CoV-2 variants demonstrated that an RBD-binding peptide was able to enhance the neutralization potency of a high-affinity nAb >100-fold. Moreover, this peptide–IgG was able to neutralize variants that were resistant to the same nAb in the bivalent IgG format, including the dominant B.1.1.529 (Omicron) variant that is resistant to most clinically approved therapeutic nAbs. To show that this approach is general, we fused the same peptide to a clinically approved nAb drug and showed that it enabled the neutralization of a resistant variant. Taken together, these results establish minimal peptide fusions as a modular means to greatly enhance affinities, potencies, and breadth of coverage of nAbs as therapeutics for SARS-CoV-2.



## INTRODUCTION

SARS-CoV-2 has become endemic, necessitating development of various COVID-19 treatment strategies beyond vaccines.<sup>1</sup> To a large extent, this is due to emergent variants of concern (VoC) that have proven to be more infectious and partially resistant to approved vaccines.<sup>2–4</sup> Consequently, there is an urgent need for alternative therapeutic strategies to complement vaccine campaigns.

SARS-CoV-2 uses its surface spike glycoprotein (S-protein) to interact with host surface receptors and enter host cells. The virus surface displays 25–100 copies of the S-protein homotrimer. Each S-protein contains two subunits: the N-terminal subunit (S1) that mediates host cell recognition and the C-terminal subunit (S2) that mediates membrane fusion.<sup>5</sup> The S1 subunit itself contains an N-terminal domain (NTD) followed by a receptor-binding domain (RBD)<sup>6</sup> that interacts with the host cell–surface protein angiotensin-converting enzyme 2 (ACE2) to initiate infection.<sup>7</sup>

Most natural neutralizing antibodies (nAbs) target the S1 subunit. Many of these bind to the RBD and compete with ACE2,<sup>8–14</sup> but a distinct subset has been shown to target a

neutralizing epitope on the NTD.<sup>9</sup> Several natural nAbs have been produced recombinantly and engineered further to develop therapeutics to treat SARS-CoV-2 infection in patients.<sup>15</sup> However, the current approved antibody drugs must be administered at very high doses and have proven to be ineffective against many VoC that have arisen since the original COVID-19 outbreak.<sup>2,4</sup> Indeed, most VoC that resist the current therapeutic nAbs contain mutations within the RBD that disrupt binding to the nAbs<sup>2</sup> but not to ACE2.<sup>16</sup> Notably, the B.1.1.529 (Omicron) variant, which emerged in South Africa and contains numerous RBD mutations, is particularly resistant to vaccination and clinical nAbs.

To address these limitations on the potency and breadth of coverage of current bivalent IgG therapies, several groups have

Received: May 9, 2022

Accepted: June 3, 2022

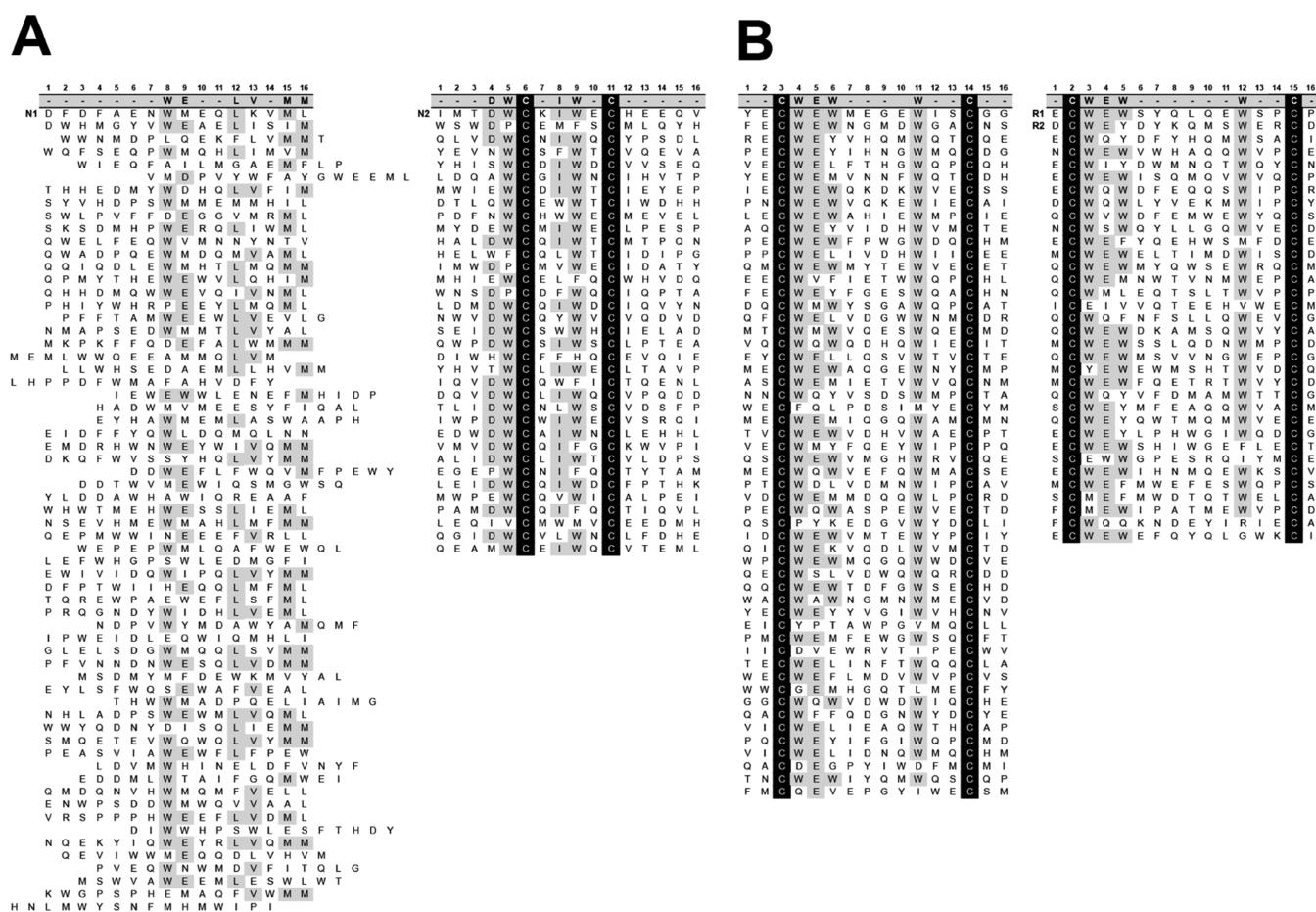


**Figure 1.** Sequence alignments of phage-derived S-protein-binding peptides. (A) Peptides selected for binding to the S-protein ECD originated from either the  $X_{16}$  library (left) or the  $C-X_4-C$  library (right). (B) Peptides selected for binding to the S-protein RBD originated from either the  $C-X_{10}-C$  library (left) or the  $C-X_{12}-C$  library (right). The positions are numbered at the top, followed by the consensus sequence for positions that exhibited high sequence conservation (>25% for  $X_{16}$ , >50% for others), and the unique selected sequences are aligned below the numbering and consensus. Sequences that match the consensus are shaded gray, and fixed cysteines are shaded black. Peptides that were characterized in detail (N1, N2, R1, R2) are labeled and shown at the top of each alignment.

developed higher valence protein-based inhibitors.<sup>17</sup> These include small modular Ab domains or non-Ab scaffolds that can be assembled as multimers with enhanced potency due to simultaneous engagement with all three RBDs on an S-protein trimer.<sup>18,19</sup> Alternatively, we have shown that the fusion of additional Fab arms to either the N- or C-terminus of an IgG heavy chain results in tetravalent IgG-like molecules with enhanced potency and effectiveness against VoC that resist bivalent IgGs.<sup>20</sup>

Notably, small peptides that target the S-protein with submicromolar affinities have been developed and have shown promise as diagnostic tools.<sup>21</sup> Here, we explored whether synthetic peptides that bind to the S-protein could be used to augment the neutralization potency of IgGs in the form of tetravalent peptide–IgG fusions that combine the binding sites of potent nAbs with the small, modular binding sites of peptides. We used naive phage-displayed peptide libraries to derive synthetic peptides that bind to neutralizing epitopes on the RBD or the NTD. We showed that these small peptides could be fused to a moderate-affinity nAb to develop peptide–IgG fusions with affinities enhanced by over 2 orders of magnitude. Most importantly, one such peptide fusion was able to greatly enhance the neutralization potency against SARS-CoV-2 and VoC—including the Omicron variant—for a high-

affinity nAb we had engineered earlier<sup>20</sup> and also for a clinically approved therapeutic nAb developed by others.<sup>10</sup> Thus, these synthetic peptides hold great promise to enhance the potency and breadth of coverage of therapeutic nAbs against SARS-CoV-2 and its VoC.

## RESULTS

**Isolation and Characterization of S-Protein-Binding Peptides.** To isolate novel peptides that bind to the S-protein of SARS-CoV-2, we used phage-displayed libraries of 16-residue peptides. We pooled together phage representing a panel of 10 peptide libraries in which diversified positions were encoded by an equimolar mixture of 19 codons representing all genetically encoded amino acids except cysteine. An “unconstrained” library ( $X_{16}$ ) contained 16 diversified positions with no fixed positions,<sup>22</sup> whereas the remaining libraries contained 14 diversified positions and two fixed cysteine residues separated by 4–12 diversified positions. These “constrained” libraries were designed to display peptides containing disulfide-bonded loops, which promote tertiary structures that can enhance binding to proteins.<sup>23</sup>

Phages representing the pooled libraries were cycled through five rounds of binding selections with immobilized S-protein ectodomain (ECD) trimer or RBD (unless otherwise noted,

virus proteins were from the B.1 variant), and several hundred clones were analyzed for binding to the ECD. Clones that exhibited strong binding signals in phage ELISAs with the ECD and negligible signals with bovine serum albumin (BSA) and neutravidin (NAV) were subjected to DNA sequence analysis. This process yielded 160 and 128 unique peptide sequences from the ECD and RBD selections, respectively. Alignment of the sequences revealed that most (85%) of the ECD-selected peptides were derived from two libraries: 63% from the X<sub>16</sub> library and 22% from the C-X<sub>4</sub>-C library (Figure 1A). In contrast, most (69%) of the RBD-selected peptides were from two different libraries: 42% from the C-X<sub>10</sub>-C library and 27% from the C-X<sub>10</sub>-C library (Figure 1B). Inspection of the aligned sequences revealed significant homology within each peptide family, which enabled us to derive consensus motifs (Figure 1). Notably, the peptides derived from the C-X<sub>10</sub>-C and C-X<sub>12</sub>-C libraries exhibited similar consensus motifs, suggesting that they bind to the S-protein in a similar manner.

For more detailed characterization, we chose four peptides that closely matched the consensus motifs for their respective families. These included a peptide from the X<sub>16</sub> library (N1) and a peptide from the C-X<sub>4</sub>-C library (N2), which were selected for binding to the ECD, and two peptides (R1 and R2) from the C-X<sub>12</sub>-C library, which were selected for binding to the RBD (Figure 1). As expected, phage ELISAs showed that all four peptide phages bound to immobilized ECD, but only peptides R1 and R2 bound to immobilized RBD (Figure 2A). To further define where each peptide bound, we assessed

whether the binding of peptide phage to the ECD could be blocked by nAbs that recognized known epitopes on either the N-terminal domain (NTD) (IgGs 5–24 and 4–8)<sup>9</sup> or the RBD (IgGs 15033-7 and REGN10933).<sup>10,20</sup> Binding of peptide phages N1 and N2, but not R1 and R2, was blocked by the two antibodies that bound to a neutralizing epitope on the NTD but not by those that bound to the ACE2-binding site of the RBD. Conversely, the binding of peptide phages R1 and R2, but not N1 and N2, was blocked by the two antibodies that bound to the RBD but not by those that bound to the NTD (Figure 2B). Taken together, these results showed that peptides N1 and N2 likely bind to the NTD, whereas peptides R1 and R2 bind to the RBD, and all peptides likely bind to sites that overlap with epitopes of nAbs.

**Optimization of S-Protein-Binding Peptides.** We took advantage of the large families of related sequences to design biased peptide-phage libraries to further optimize peptides N1 and R1 (Figure 3). For each peptide, we used the sequence logo derived from its family to identify highly conserved positions that were fixed, and variable positions, which were randomized using degenerate codons to encode a mix of parent and other amino acids that were prevalent in the sequence logo. Phage pools representing each biased library were cycled through five rounds of selection for binding to the S-protein ECD trimer, positive clones were identified by phage ELISA, and DNA sequencing revealed 86 and 25 unique sequences from the N1 and R1 libraries, respectively (Figure 4). We used the unique sequences to derive a sequence logo for each selection pool (Figure 3). We chose unique peptide sequences that closely matched the logo for further characterization, reasoning that these likely represented high-affinity binders.

Based on this process, we identified four variants of peptide N1 (N1a, b, c, d) and two variants of peptide R1 (R1a, b) for chemical synthesis (Figure 4). These were synthesized as 22-residue peptides consisting of the following: a Gly residue, followed by the selected 16-residue sequence, followed by a 5-residue hydrophilic linker (Gly–Gly–Lys–Gly–Lys), followed by biotin. We used biolayer interferometry (BLI) to determine binding kinetics and affinities. Biotinylated peptides were immobilized on sensor chips that were incubated with solution-phase S-protein ECD (Figure S1). Peptide N1 did not exhibit detectable binding, presumably due to low affinity, but its variants bound with moderate apparent affinities (apparent  $K_D = 26–68$  nM). Peptide R1 and its variants exhibited high apparent affinities in the single-digit nanomolar range for the S-proteins from both the B.1 variant (apparent  $K_D = 0.8–5.6$  nM) and the B.1.1.529 variant (apparent  $K_D = 3–7$  nM) (Table 1). We note that polyvalent avidity effects likely enhance these apparent affinities, and the intrinsic monovalent affinities are likely lower. Nonetheless, this format does mimic the polyvalent nature of the virus-neutralizing molecules we ultimately intended to produce, as described below.

**Production and Characterization of Peptide–IgG Fusions.** We next explored whether peptide fusions could enhance the affinity of a neutralizing IgG targeting the ACE2-binding site of the RBD. For this purpose, we used the moderate-affinity IgG 15033 that we had selected from a naïve phage-displayed synthetic antibody library<sup>20</sup> to accurately discern affinity differences. Peptide N1 or R1 was fused to the N-terminus of either the light chain (LC) or heavy chain (HC) of IgG 15033 with an intervening 20-residue Gly/Ser linker (Figure S2). The resulting peptide–IgG fusion proteins

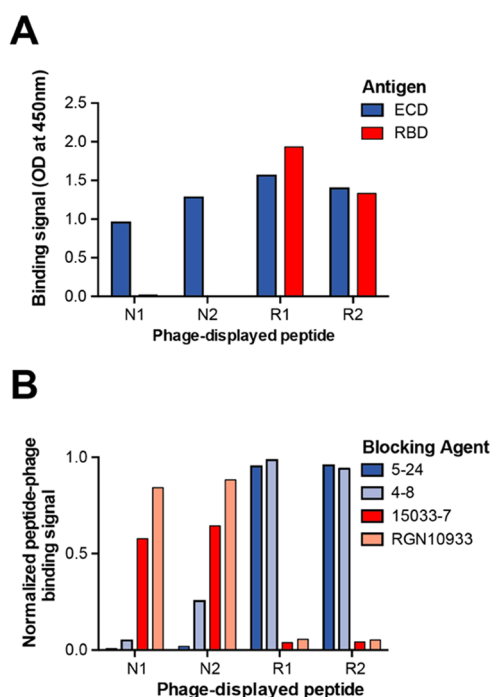


**Figure 2.** Characterization of epitopes for phage-displayed S-protein-binding peptides. (A) Phage ELISAs for peptide-phage binding to immobilized S-protein ECD (blue bars) or RBD (red bars). Binding was quantified by the optical density at 450 nm (y-axis) for 0.5 nM phage, displaying the indicated peptide (x-axis). (B) Phage ELISAs for peptide-phage (x-axis) binding to the immobilized S-protein ECD in the presence of saturating concentrations of antibodies that bind to the NTD (5–24, dark blue; 4–8, light blue) or RBD (15033-7, dark red; RGN10933, light red). The binding signal (y-axis) was normalized to binding in the absence of an antibody.

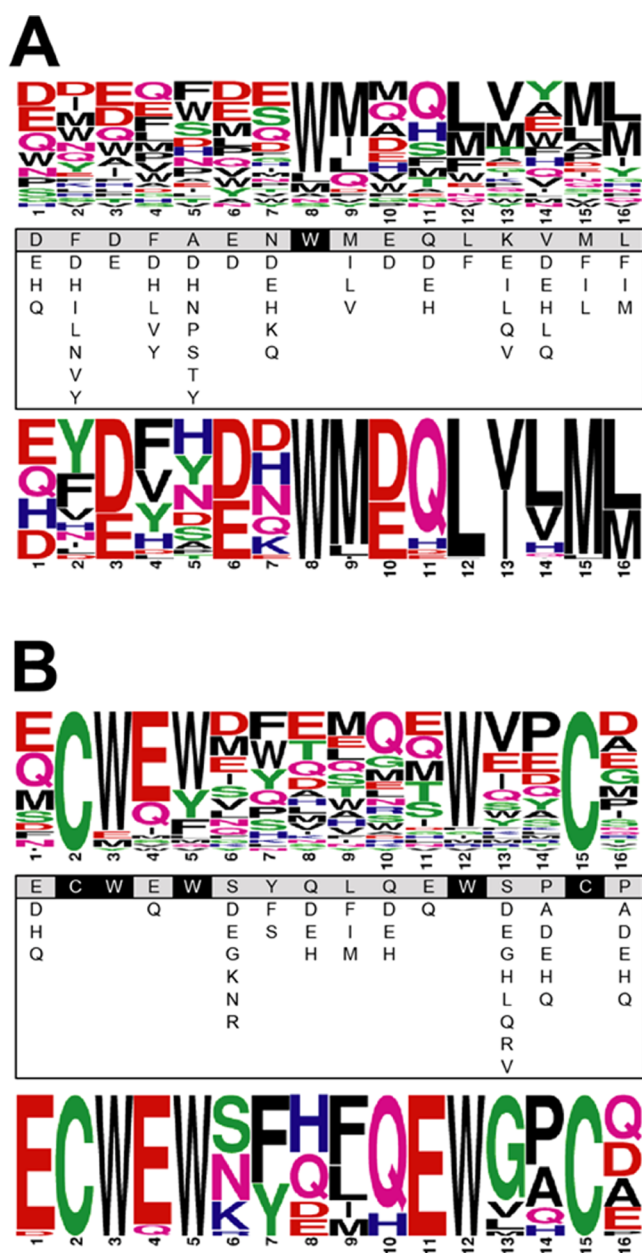


**Figure 3.** Optimization of S-protein-binding peptides. Biased peptide-phage libraries were designed to optimize (A) peptide N1 or (B) peptide R1. For each peptide, the sequence logo at the top was derived from the family of peptides selected from naive peptide-phage libraries (Figure 1). Below the logo, the parent peptide sequence is shown with positions that were fixed or diversified shaded black or gray, respectively. For each diversified position, additional amino acids present in the displayed library are shown below the parent amino acid. Output clones obtained from selection of the biased library against the S-protein ECD were used to construct the sequence logo at the bottom of each panel (Figure 4).

and IgG 15033 were purified by transient transfection in mammalian Expi293F cells.<sup>20</sup> All proteins could be purified to near-homogeneity by affinity chromatography with protein-A resin, as evidenced by SDS-PAGE (Figure 5A). As expected, under nonreducing conditions, the single bands for the intact peptide–IgG molecules migrated slightly slower than the band for IgG 15033. Under reducing conditions, either the HC band or the LC band migrated slower for peptide–IgG fusions compared with that for IgG 15033, as expected for HC or LC

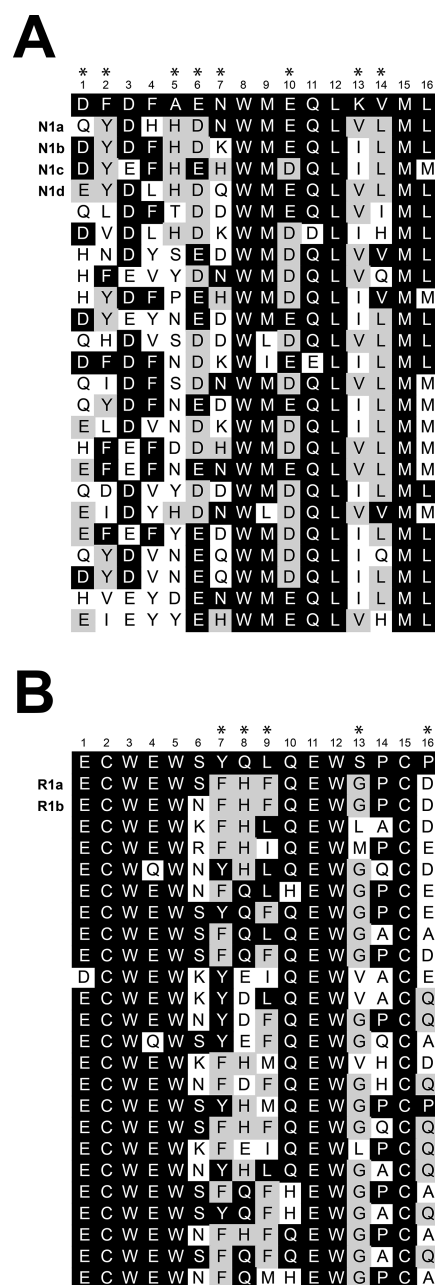


**Figure 4.** Sequence alignments of S-protein-binding peptides derived from biased phage-displayed libraries. Peptides selected for binding to the S-protein ECD originated from the biased library based on the sequence of (A) peptide N1 or (B) peptide R1 (see Figure 3). Only a subset of peptides from the N1 selection is shown. The positions are numbered at the top, followed by the sequence of the parent peptide. Amino acids that match the parental sequence at each position are shaded black. Amino acids that do not match the parental but are most prevalent at each position are shaded gray. Asterisks indicate positions at which sequences diverged from the parental sequence, suggesting that sequence differences here may enhance the affinity of the variants relative to the parent. The sequences of peptide variants chosen for chemical synthesis and further characterization are labeled to the left of each alignment.

peptide fusions, respectively. Like IgG 15033 and the highly specific IgG trastuzumab, the four peptide–IgG fusions did not bind to seven immunized, heterologous proteins that are known to exhibit high nonspecific binding to some IgGs

Table 1. Kinetics of Synthetic Peptide Binding to S-Protein ECD<sup>a,b,c</sup>

Peptide	Sequence <sup>a</sup>																$k_{on}$ ( $10^2$ M <sup>-1</sup> s <sup>-1</sup> )	$k_{off}$ ( $10^{-6}$ s <sup>-1</sup> )	$K_D$ (nM) <sup>b</sup>						
	1	2	3	4	5	6	7	8	9	10	11	12	13	14	15	16									
N1	G	D	F	D	F	A	E	N	W	M	E	Q	L	K	V	M	L	G	G	K	G	K	N.D.	N.D.	<sup>c</sup> N.D.
N1a	-	Q	Y	-	H	H	D	-	-	-	-	-	-	V	L	-	-	-	-	-	-	-	160 ± 3	400 ± 10	26 ± 1
N1b	-	-	Y	-	-	H	D	K	-	-	-	-	I	L	-	-	-	-	-	-	-	-	99 ± 1	360 ± 3	36 ± 1
N1c	-	-	Y	E	-	H	-	H	-	-	D	-	I	L	-	M	-	-	-	-	-	-	93 ± 2	630 ± 10	68 ± 2
N1d	-	E	Y	-	L	H	D	Q	-	-	-	-	V	L	-	-	-	-	-	-	-	-	140 ± 4	870 ± 10	61 ± 2
R1	G	E	C	W	E	W	S	Y	Q	L	Q	E	W	S	P	C	P	G	G	K	G	K	430 ± 4 (700 ± 30)	150 ± 5.0 (460 ± 1)	3.4 ± 0.1 (6.6 ± 1)
R1a	-	-	-	-	-	-	-	F	H	F	-	-	G	-	D	-	-	-	-	-	-	-	430 ± 4 (1300 ± 20)	130 ± 5.5 (420 ± 9)	3.1 ± 0.1 (3.2 ± 1)
R1b	-	-	-	-	-	N	F	H	F	-	-	G	-	D	-	-	-	-	-	-	-	-	560 ± 6 (1400 ± 20)	100 ± 5.5 (370 ± 9)	1.8 ± 0.1 (2.6 ± 1)

<sup>a</sup>Peptides were synthesized with a C-terminal biotin group. The 16-residue sequence selected for binding to the S-protein ECD or RBD is shaded gray and numbered as in Figures 1 and 4. For optimized variants of peptide N1 (N1a, b, c, d) and peptide R1 (R1a, b), dashes indicate the identity with the parent amino acid. A biotin tag was added to the C-terminus of each peptide for capture on streptavidin-coated sensors. <sup>b</sup>Kinetic binding constants ( $k_{on}$  and  $k_{off}$ ) and the equilibrium dissociation constant ( $K_D$ ) were determined by the global fitting of response traces obtained when dipping peptide-coated sensors into solutions of S-protein. For R1, values in parentheses were determined from measurements against B.1.1.529 S-protein. <sup>c</sup>N.D., not determined. Affinity for the CoV-2-spike was too low to be measured by BLI.

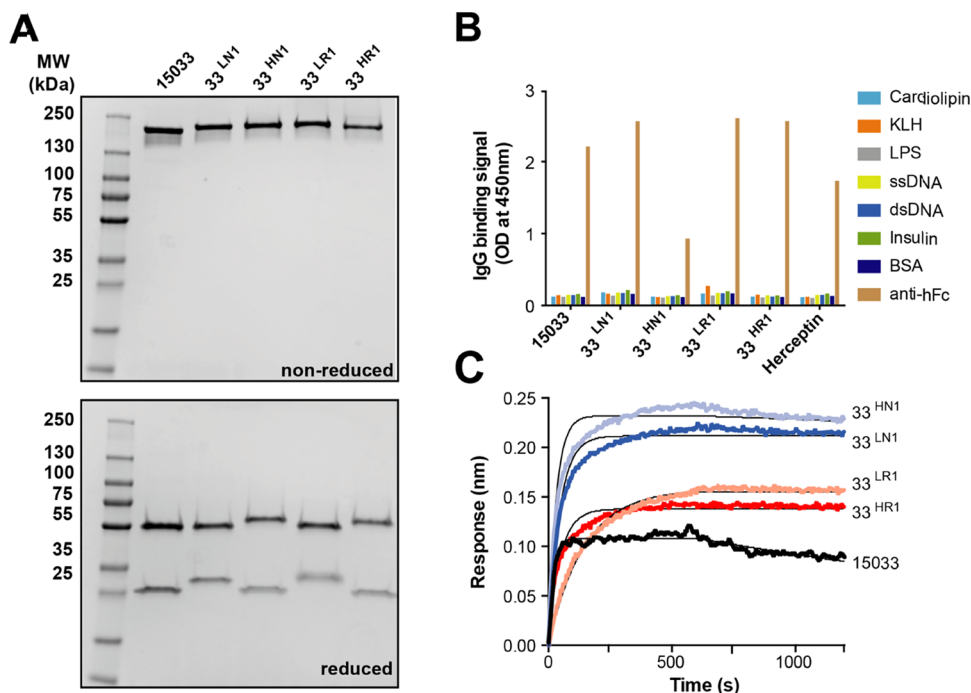


**Figure 5.** Characterization of peptide-IgG fusion proteins. Peptides were fused to the N-terminus of the HC or LC of IgG 15033, and the resulting peptide-IgG fusions were named as follows: N1 fused to HC, 33<sup>HN1</sup>; N1 fused to LC, 33<sup>LN1</sup>; R1 fused to HC, 33<sup>HR1</sup>; and R1 fused to LC, 33<sup>LR1</sup>. (A) SDS-PAGE analysis of peptide-IgG fusion proteins under nonreducing (top) or reducing conditions (bottom). (B) Assessment of nonspecific binding of peptide-IgG fusion proteins to immobilized antigens or a goat antihuman Fc Ab (positive control). (C) BLI sensor traces for 20 nM IgG 15033 or peptide-IgG fusions binding to the immobilized S-protein ECD. Association and dissociation kinetics were monitored for 600 seconds each. The derived binding constants are shown in Table 2.

(Figure 5B). Lack of binding in this assay is a predictor of good pharmacokinetics *in vivo*.<sup>24</sup>

Kinetic binding analysis by BLI showed that the tetravalent peptide-IgG fusions exhibited greatly reduced off-rates compared with IgG 15033 (Figure S3), and consequently, affinities for the S-protein ECD were greatly improved (Figure 5C and Table 2). These results were as expected since the addition of a peptide ligand to an RBD-binding IgG should reduce the overall free energy of binding and thus increase the binding efficiency. In particular, the peptide-IgG with peptide

R1 fused to its HC (33<sup>HR1</sup>) and the peptide-IgG with peptide N1 fused to its LC (33<sup>LN1</sup>) exhibited extremely slow off-rates that were beyond the sensitivity of the instrument, and consequently, the apparent dissociation constants were estimated to be subpicomolar (apparent  $K_D$  < 1 pM), which was >100-fold improved relative to IgG 15033 (apparent  $K_D$  = 100 pM). We note that the response signals of the N1 peptide-IgG fusions were much greater than those of the R1 peptide-IgG fusions. This is likely due to peptide N1 being unconstrained with a higher  $k_{off}$  for the S-protein compared to

**Table 2. Kinetics of Peptide–IgG Fusion Protein Binding to S-Protein ECD**

IgG <sup>a</sup>	$k_{\text{on}}$ ( $10^4 \text{ M}^{-1} \text{ s}^{-1}$ )	$k_{\text{off}}$ ( $10^{-6} \text{ S}^{-1}$ )	$K_{\text{D}}$ (pM) <sup>b</sup>
15033	170 ± 5	500 ± 20	300 ± 20
33 <sup>HN1</sup>	160 ± 5	38 ± 20	24 ± 10
33 <sup>LN1</sup>	110 ± 3	<0.1	<1
33 <sup>HR1</sup>	120 ± 4	<0.1	<1
33 <sup>LR1</sup>	35 ± 1	2.2 ± 1	6.1 ± 3

<sup>a</sup>Peptide–IgG fusion proteins consisted of phage-derived peptides fused to the N-terminus of the light chain or heavy chain of IgG 15033. The following nomenclature was used: L, light-chain fusion; H, heavy-chain fusion; N1, NTD-binding peptide 1; and R1, RBD-binding peptide 1 (see Table 1 for sequences). <sup>b</sup>Kinetic binding constants ( $k_{\text{on}}$  and  $k_{\text{off}}$ ) and the equilibrium dissociation constant ( $K_{\text{D}}$ ) were determined by the global fitting of response traces obtained when dipping S-protein-coated sensors into solutions of indicated IgG.

R1 (Table 1). This may allow the N1 peptide–IgG fusions to adopt more extended conformations upon interaction with the S-protein, which would manifest as greater signals in the BLI experiment.

**Inhibition of Virus Infection in Cell-Based Assays.** To assess the efficacy of the peptides and peptide–IgG fusion proteins for the neutralization of SARS-CoV-2 VoC, we first used mammalian cell infection assays with pseudoviruses consisting of HIV-gag-based, lentivirus-like particles pseudotyped with the SARS-CoV-2 S-protein.<sup>25</sup> Neither peptide, nor their optimized variants, exhibited any effect on pseudovirus infection at concentrations up to 10  $\mu\text{M}$  (Figure 6A). However, peptide–IgG fusion proteins with the N1 peptide or the R1 peptide fused to the N-terminus of the HC (33<sup>HN1</sup> or 33<sup>HR1</sup>, respectively) or LC of IgG 15033 (33<sup>LN1</sup> or 33<sup>LR1</sup>, respectively) exhibited enhanced neutralization potency compared with the IgG alone (Figure 6B).

Finally, we explored the critical question of whether peptide fusions could enhance potency of nAbs against authentic SARS-CoV-2 in ACE2 expressing Vero E6 cell-based assays. For this purpose, we fused peptide R1 to the N-terminus of the HC of IgG 15033-7, a more potent variant of IgG 15033 with an optimized LC.<sup>20</sup> Neutralization efficiency of the resulting peptide–IgG fusion protein (33-7<sup>HR1</sup>) was compared to IgG 15033-7 against a panel of seven SARS-CoV-2 variants: Wuhan (B.1), Italy (B.1.1), the United Kingdom (B.1.1.7), South Africa (B.1.351 and B.1.529), Nigeria (B.1.525), and Brazil (B.1.128). In every case, the potency of the peptide–IgG fusion greatly exceeded that of the IgG (Figure 7A). Indeed, peptide–IgG 33-7<sup>HR1</sup> neutralized three VoC in the single-digit ng/mL range ( $\text{IC}_{50} = 6.5\text{--}7.6 \text{ ng/mL}$ ), and three other VoC in the double-digit ng/mL range ( $\text{IC}_{50} = 12\text{--}49 \text{ ng/mL}$ ). Notably, 33-7<sup>HR1</sup> was even able to neutralize the B.1.1.529 variant, which is resistant to most clinically approved IgG drugs, albeit with reduced potency ( $\text{IC}_{50} = 260 \text{ ng/mL}$ ). In contrast, IgG 15033-7 was less effective than IgG 33-7<sup>HR1</sup> against three VoC ( $\text{IC}_{50} = 64\text{--}310 \text{ ng/mL}$ ), much less effective against three other VoC ( $\text{IC}_{50} > 900 \text{ ng/mL}$ ), and completely ineffective against B.1.1.529.

We also explored whether the modularity of the peptides could be exploited to enhance the potency of a clinically approved therapeutic nAb (REGN10933; Figure 7B). We constructed a variant of REGN10933 by fusing peptide R1 to the N-terminus of the HC. The resulting peptide–IgG fusion (REGN10933<sup>HR1</sup>) proved to be more potent than

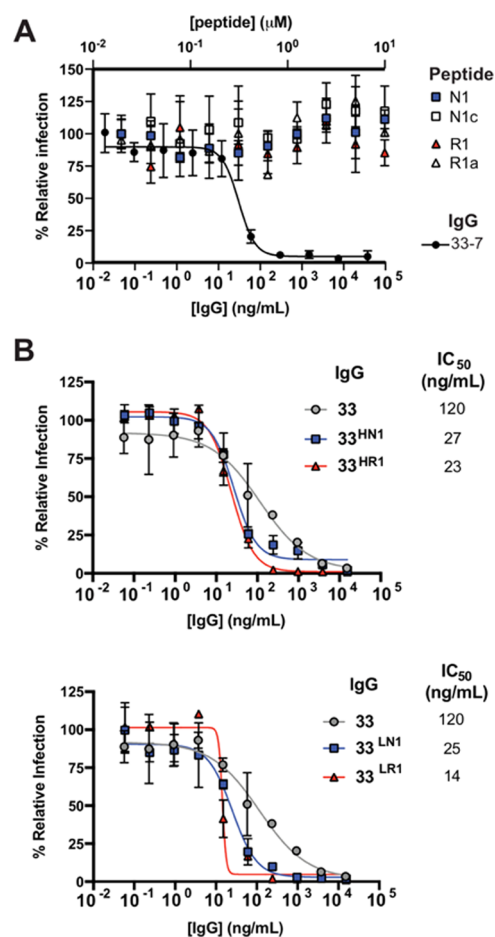


**Figure 6.** Neutralization of SARS-CoV-2 pseudovirus. Neutralization assays were conducted with HIV-gag-based, lentivirus-like particles pseudotyped with the S-protein of the original B.1 strain from Wuhan. (A) Assays were conducted with synthetic peptides N1 (blue squares), R1 (red triangles), or the highest affinity optimized peptide for each (clear square and triangle, respectively) and IgG 15033-7 (black circle) as a positive control. (B) Assays were conducted with IgG 15033 (gray circle) or with peptide–IgG 33<sup>HN1</sup> (blue square), 33<sup>HR1</sup> (red triangle, upper), or 33<sup>LN1</sup> (blue square), 33<sup>LR1</sup> (red triangle, lower).

REGN10933 in neutralization assays against the SARS-CoV-2 variant D614G ( $\text{IC}_{50} < 10$  or  $\sim 10 \text{ ng/mL}$ , respectively). Most strikingly, peptide–IgG REGN10933<sup>HR1</sup> was also extremely potent against the South African variant B.1.351 ( $\text{IC}_{50} < 10 \text{ ng/mL}$ ), against which REGN10933 was completely ineffective ( $\text{IC}_{50} > 1000 \text{ ng/mL}$ ), consistent with previous reports.<sup>2</sup> Taken together, these results showed that peptide fusions greatly enhanced the potency and breadth of coverage of neutralizing IgGs against SARS-CoV-2 and its VoC.

## DISCUSSION

The trimeric structure of the SARS-CoV-2 S-protein can be exploited to engineer Ab-based inhibitors with enhanced neutralization by engaging three neutralizing epitopes on a single trimer. Structural studies from us and others have shown that potent neutralizing IgGs engage two RBDs on an S-protein trimer,<sup>26</sup> and we have shown that the addition of Fab arms to either end of an IgG can further enhance neutralization by enabling engagement to the third RBD.<sup>20</sup> Here, rather than

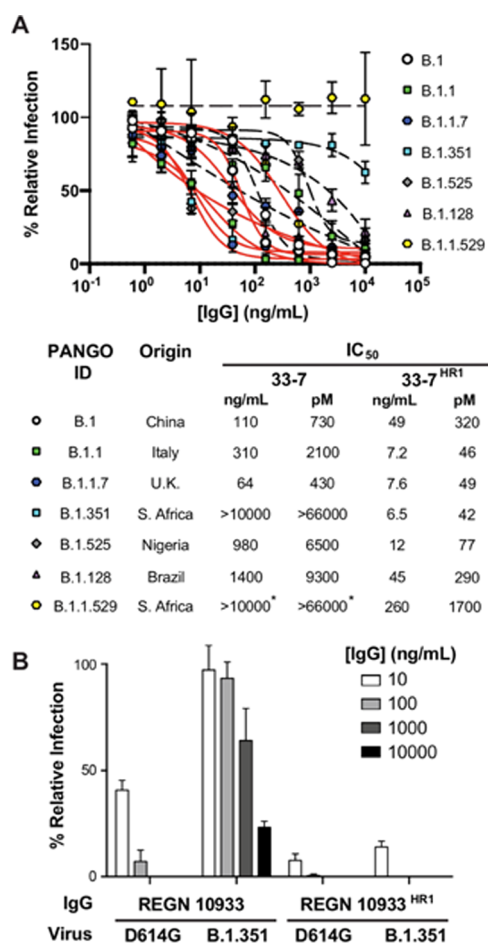


**Figure 7.** Neutralization of SARS-CoV-2 variants. (A) Authentic virus neutralization assays to test the efficacy of IgG 15033-7 and peptide–IgG 33-7<sup>HR1</sup> (IgG 15033-7 with peptide R1 fused to the N-terminus of its HC) against isolated SARS-CoV-2 variants. The virus was pretreated with serial dilutions of IgG, followed by infection of ACE2-expressing Vero E6 cells, and measured relative to the untreated control. At the top, the graph shows the neutralization curves for seven SARS-CoV-2 variants treated with IgG 15033-7 (black dashed lines) or peptide–IgG 33-7<sup>HR1</sup> (red solid lines). At the bottom, the table shows the symbols used for the curves and the country of origin for each virus variant. IC<sub>50</sub> values calculated from the curves are shown in ng/mL or nM units. (B) Focus reduction neutralization assays to test the efficacy of IgG REGN10933 and peptide–IgG REGN10933<sup>HR1</sup> (REGN10933 with peptide R1 fused to the N-terminus of its HC) against isogenic SARS-CoV-2 variants D614G and B.1.351. The virus was pretreated with serial dilutions of IgG followed by infection of ACE2-expressing Vero E6 cells, which was measured relative to the untreated virus. Each value represents the mean of duplicate measurements.

using large Fabs as the additional binding domain, we used small peptides to greatly enhance the affinities and potencies of tetravalent peptide–IgG fusions compared with our bivalent IgG 15033-7. Most importantly, peptide–IgG 33-7<sup>HR1</sup> acted as a potent inhibitor of virus variants that resisted IgG 15033-7 (Figure 7A). Indeed, we showed further that a peptide–IgG version of the approved drug REGN10933 was able to potently neutralize a VoC against which REGN10933 was completely ineffective (Figure 7B).

To gain insight into the structural basis for how a peptide within a peptide–IgG fusion could enhance affinity, we examined our published model of two 15033-7 Fabs bound

to the S-protein trimer, reasoning that this likely provides an accurate view of how the two Fab arms of a bivalent IgG would bind (Figure 8A). In this model, the RBDs bound to Fabs are in an “up” conformation, whereas the unbound RBD is in a “down” conformation. The C-termini of the two Fab HCs are separated by 45 Å and are well positioned to be linked to an Fc in an IgG molecule, whereas their N-termini are close to the unbound RBD. In particular, the N-terminus of one HC is 45 Å from the center of the exposed region of the neutralizing epitope for Fab 15033-7 on the unbound RBD. Although peptide R1 alone does not appear to neutralize virus infection (Figure 6A), it likely binds to a site that overlaps with this epitope, given that the peptide and IgG compete for binding to the S-protein (Figure 2B). Consequently, in peptide–IgG 33-7<sup>HR1</sup> with two Fabs bound to an S-protein trimer, it is reasonable to assume that one of the R1 peptides could bind simultaneously to a region close to this third epitope, and the estimated length (~70 Å) of the extended 20-residue linker that connects the peptide to the IgG is consistent with this model.

We next examined an analogous structural model of two REGN10933 Fabs bound to an S-protein trimer (Figure 8B). The epitopes for REGN10933 and 15033-7 Fabs share a significant overlap, but the REGN10933 Fabs are oriented such that the N-termini of the two HCs are 34 or 66 Å from the 15033-7 epitope on the unbound RBD. Consequently, the ~70 Å linker that connects each peptide to the IgG would be sufficient to enable either of the two fused peptides within peptide–IgG10933<sup>HR1</sup> to bind to a site close to this epitope.

We also developed peptides that bound to the NTD, likely at a site that overlaps with epitopes for other neutralizing nAbs (Figure 2B). We showed that peptide N1 greatly enhanced the affinity of peptide–IgG 33<sup>LN1</sup>, and both peptide–IgG 33<sup>LN1</sup> and 33<sup>HR1</sup> exhibited enhanced potency in a pseudovirus neutralization assay (Figure 6B). Notably, peptides R1 and N1 appear to work best as fusions to the HC or LC, respectively, and given that they recognize completely distinct epitopes, it will be interesting to explore whether dual fusions of the two peptides could enhance the potencies of peptide–IgG fusions even further, and these studies are ongoing.

The ultimate value of peptide–IgG fusions targeting SARS-CoV-2 and its variant resides in the potential for the development of superior therapeutics for the treatment of COVID-19 and other viral diseases. We are currently assessing and optimizing the biophysical properties of the peptide–IgG fusions with the aim of developing drug-grade biologics. However, there is already a strong precedent for peptide–IgG fusions as clinical drugs in the form of biologics that have reached phase 2 clinical trials as cancer therapeutics.<sup>27</sup> These anticancer biologics are very similar in format to the antiviral peptide–IgG fusions we report here.<sup>28</sup> Critically, anticancer peptide–IgG fusions have exhibited good pharmacokinetic profiles<sup>29</sup> and tissue penetration,<sup>30</sup> and they have been well tolerated in the clinic.<sup>31</sup> Taken together, our results establish peptide–IgG fusions as a powerful means for greatly enhancing the potency and coverage of next-generation biologics for the treatment of diseases caused by SARS-CoV-2 and its variants.

## MATERIALS AND METHODS

**Protein Production.** The SARS-CoV-2 S-protein ECD and RBD were produced and purified as described<sup>20</sup> and were a kind gift from Dr. James Rini. Purified proteins were site-specifically biotinylated in a reaction with 200 μM biotin, 500 μM ATP, 500 μM MgCl<sub>2</sub>, 30 μg/

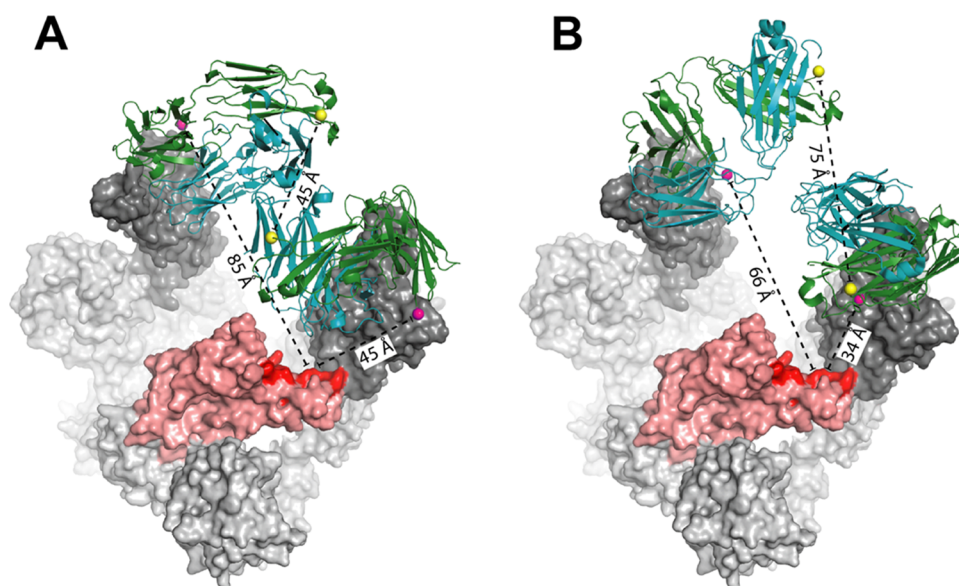


**Figure 8.** Structural models of multivalent ligands binding to the S-protein trimer. Structural models are shown for (A) two 15033-7 Fabs or (B) two RGN10933 Fabs bound to the S1 subunit of the S-protein of SARS-CoV-2. The S1-protein is shown as a surface colored in light gray, except for the following regions. The bound RBDs in the “up” position are colored dark gray. The unbound RBD in the “down” position is colored dark or light red for residues that are within or outside the epitope for Fab 15033-7, respectively. The Fabs are shown as ribbons, with the HC and LC colored forest green or teal, respectively. The C-termini and N-termini of the Fab HCs are shown as yellow or magenta spheres, respectively. Distances are shown as dashed black lines and are labeled accordingly.

mL BirA, 0.1% (v/v) protease inhibitor cocktail, and not more than 100  $\mu$ M of the protein–AviTag substrate. The reactions were incubated at 30 °C for 2 h, and biotinylated proteins were purified by size-exclusion chromatography.

**Antibody Production.** IgG and peptide–IgG fusion proteins were produced as described.<sup>20</sup> S-protein-binding peptides were fused to the N-terminus of the heavy or light chain through a 20-residue linker (sequence: GGGGSGGGGSGGGGSGGGG) using standard molecular biology techniques.

**Phage Display Selections.** Naïve libraries were constructed as described.<sup>22</sup> For libraries for peptide optimization, oligonucleotides were synthesized using degenerate codons encoding for the amino acids at each position indicated in Figure 3. Oligonucleotide-directed mutagenesis was performed to introduce randomized sequences fused to the gene-8 major coat protein of M-13 bacteriophage, as described.<sup>32</sup> Each phage-displayed peptide library was selected for binding to the immobilized S-protein ECD or RBD, as described,<sup>32</sup> but with the following modifications. Biotinylated S-protein ECD or RBD was captured on wells coated with NAV, followed by incubation with the phage-displayed peptide library. After five rounds of binding selections, individual clones were picked and DNA was sequenced. Clones that showed a significant binding signal to S-protein ECD and/or RBD, but not to BSA or NAV, were selected for further analysis.

**Peptide Synthesis.** Peptides were synthesized by AbClonal. Peptide sequences selected by phage display (gray shading in Table 1) were synthesized with a Gly residue added to the N-terminus and a Gly–Gly–Lys–Gly–Lys linker added to the C-terminus. Biotin was conjugated via the C-terminal lysine residue.

**ELISAs.** Phage ELISAs were performed, as described,<sup>20</sup> but with the following modifications: 384-well Maxisorp plates (Sigma-Aldrich) were coated with NAV, or left uncoated as a negative control, and blocked with PBS, 0.5% bovine serum albumin (BSA). Biotinylated target protein was captured by incubation in NAV-coated and BSA-blocked wells, or with buffer solution alone as a negative control, at room temperature. For competition ELISAs, blocking IgG was incubated with coated and blocked wells for 1 h at room temperature. Wells were incubated with peptide phage in PBS, 0.5% BSA for 1 h. Plates were washed, incubated with anti-M-13-HRP antibody (Sino Biological, catalog number 11973-MM05T-H), and

developed with TMB substrate (Mandel, catalog number KP-50-76-03).

For assessing the specificity of antibodies (Figure 5B), the following proteins were used: KLH (Sigma-Aldrich, H8283), cardiolipin (Sigma-Aldrich, C0563), BSA (Medstore, ALB001), insulin (Sigma-Aldrich, I0516), LPS (Invivogen, tlr-eblps), ssDNA (Sigma-Aldrich, D4522), and goat antihuman Fc (Jackson Labs—109-005-098). Proteins (5  $\mu$ g/mL) were coated for 2 h at room temperature on 96-well maxisorp plates (Sigma-Aldrich), followed by blocking with 0.5% BSA in PBS for 1 h. Antibodies were applied to the blocked and coated plate for 30 min followed by washing and detection with an anti-kappa-chain-HRP conjugate (Southern Biotech, 2060-05).

**Biolayer Interferometry.** For IgGs and peptide–IgG fusions, binding kinetics for the S-protein were determined by BLI with an Octet HTX instrument (ForteBio), as described.<sup>20</sup> For peptides, biotinylated peptides (Table 1) were immobilized on streptavidin-coated sensors that were subsequently blocked with excess biotin. Following equilibration with assay buffer, the loaded biosensors were dipped for 600 s into wells containing 3-fold serial dilutions of S-protein ECD and subsequently were transferred back into the assay buffer for 600 s. Binding response data were corrected by the subtraction of response from a reference and were fitted with a 1:1 binding model using the ForteBio Octet Systems software 9.0. We determined  $K_D$  values at various peptide loading densities to ensure that high densities were not impacting kinetic measurements at the sensor.

**Sequence Alignment and Analysis.** Sequences of binding peptides were imported into Geneious R9 software (Biomatters Ltd.). Peptides were sorted based on the library from which they originated and aligned separately using the MUSCLE algorithm. In the case of peptides lacking cysteines, a strict penalty was imposed on the formation of gaps during alignment. Sequence logos were created using the weblogo server (<https://weblogo.berkeley.edu/logo.cgi>).

**Production of Pseudoviruses.** HEK-293 cells (ATCC) were seeded in a 6-well plate at  $3 \times 10^5$  cells/well in DMEM (ThermoFisher, 11995-065) supplemented with 10% FBS and 1% penicillin–streptomycin (Gibco, 15140122) and grown overnight at 37 °C with 5% CO<sub>2</sub>. HEK-293 cells were cotransfected with 1  $\mu$ g pNL4-3.luc.R-E-plasmid (luciferase-expressing HIV-1 with a defective

envelop protein) (NIH AIDS Reagent Program, ARP2128) and a 0.06  $\mu\text{g}$  CMV-promoter-driven plasmid encoding the S-protein using the Lipofectamine 2000 transfection reagent (ThermoFisher, 11668027). Pseudovirus particles were harvested by collecting the supernatant 48 h after transfection and were filter-sterilized (0.44  $\mu\text{m}$ , Millipore-Sigma, SLHA033SS).

**Pseudovirus Infection Assays.** HEK293T cells stably overexpressing the full-length human ACE2 protein were seeded in 96-well white polystyrene microplates (Corning, CLS3610) at  $3 \times 10^4$  cells/well in DMEM (10% FBS and 1% penicillin–streptomycin) and were grown overnight at 37 °C with 5% CO<sub>2</sub>. Pseudovirus particles were mixed with Ab, incubated at room temperature for 10 min, and added to the cells. The cells were incubated at 37 °C with 5% CO<sub>2</sub> and the medium was replaced with fresh DMEM (10% FBS and 1% penicillin–streptomycin) after 6 h and again every 24 h up to 72 h. To measure the luciferase signal (pseudovirus entry), DMEM was removed and DPBS (ThermoFisher) was added to cells before mixing with an equal volume of the ONE-Glo EX Luciferase Assay System (Promega, E8130). Relative luciferase units were measured using a BioTek Synergy Neo plate reader (BioTek Instruments Inc.). The data were analyzed by GraphPad Prism Version 8.4.3 (GraphPad Software, LLC).

**Authentic virus infection assays.** To evaluate the neutralization of SARS-CoV-2 VoC, the authentic isolates of USA\_WA1/2020, B.1.1.7, B.1.351, B.1.617.2, B.1.617.2+, B.1.1.529 (BA.1), and the chimeric B.1.1.28 (that was generated on the genetic background of WA1/2020) were evaluated for neutralization using a focus reduction neutralization test and potency was estimated as described.<sup>20,33,34</sup> All viruses were verified by next-generation sequencing. Alternatively, authentic SARS-CoV-2 strains were used in a microneutralization assay, as described.<sup>35</sup> In brief, serial fourfold dilutions of antibody, starting from 10  $\mu\text{g}/\text{mL}$ , were preincubated with  $10^2$  focus-forming units per 100  $\mu\text{L}$  at 37 °C for 1 h. The antibody–virus mixture was transferred to 96-well tissue culture plates containing Vero-hACE2-TMPRSS2 cell monolayers in duplicate and incubated at 37 °C and 5% CO<sub>2</sub> for 1 h; subsequently, the cells were overlaid with 1% (wt/vol) methylcellulose in MEM. Plates were harvested at 24 h by the removal of overlays and fixation for 20 min with 4% paraformaldehyde in PBS at room temperature. Plates were washed with permeabilization buffer (PBS supplemented with 0.1% saponin and 0.1% BSA) and sequentially incubated overnight with the oligoclonal pool of anti-SARS-CoV-2 Abs.<sup>9</sup> The plates with Omicron (B.1.1.529) were additionally incubated with the cross-reactive pool of Abs for SARS-CoV-1 that bind to the RBD and compete with Ab (VanBlargan et al.). The plates were incubated with HRP-conjugated antimouse (Sigma-Aldrich, A5278), goat antihuman Abs (Sigma-Aldrich, A6029), and visualized by the KPL TrueBlue substrate and quantitated by an Immunospot microanalyzer (Cellular Technologies), as described.<sup>36,37</sup>

## STRUCTURAL ANALYSIS

The model of two 15033-7 Fabs bound to the SARS-CoV-2 S-protein (PDB entry 7KMK) was imported into PyMol (DeLano Scientific, LLC). Distances between the HC N-termini and the 15033-7 epitope on the unbound RBD were measured as the distance between the C $\alpha$  of the first residue of the HC and the C $\beta$  of Tyr<sup>489</sup> of the S-protein. To build the model of two RGN10933 Fabs bound to the S-protein, the model of RGN10933 and RGN10987 bound to the RBD (PDB entry 6XDG) was imported into PyMol along with the data from PDB entry 7KMK. The data from PDB entry 6XDG were duplicated, and the RBDs of the model were superposed with the two RBDs in the “up” position in the model from PDB entry 7KMK. The RBDs in the model from PDB entry 6XDG, RGN10987 Fabs, and 15033-7 Fabs were then eliminated from the model, leaving only the two RGN10933 from PDB entry 6XDG bound to the S-protein from PDB

entry 7KMK. Distances were measured the same way as for 15033-7.

## ASSOCIATED CONTENT

### Supporting Information

The Supporting Information is available free of charge at <https://pubs.acs.org/doi/10.1021/acscchembio.2c00411>.

This includes (1) raw BLI traces of S-protein binding to immobilized R1 and N1 peptides and their variants. Data from which binding parameters were calculated is also shown overlaid with the raw traces; (2) amino acid sequences of R1 peptide fused to the light or heavy chain of the 15033-7 antibody. All CoV-2 S-protein-binding peptides were fused to antibody heavy or light chains in this manner; and (3) raw BLI traces of CoV-2 S-protein-binding peptides fused to antibody 15033 binding to the immobilized S-protein. Data from which binding parameters were calculated is also shown overlaid with the raw traces (PDF)

## AUTHOR INFORMATION

### Corresponding Author

Sachdev S. Sidhu – Department of Molecular Genetics, The Donnelly Centre, University of Toronto, MSS 3E1 Toronto, Ontario, Canada; [orcid.org/0000-0001-7755-5918](https://orcid.org/0000-0001-7755-5918); Email: [sachdev.sidhu@utoronto.ca](mailto:sachdev.sidhu@utoronto.ca)

### Authors

Jonathan M. Labriola – Department of Molecular Genetics, The Donnelly Centre, University of Toronto, MSS 3E1 Toronto, Ontario, Canada; [orcid.org/0000-0002-8486-6738](https://orcid.org/0000-0002-8486-6738)

Shane Miersch – Department of Molecular Genetics, The Donnelly Centre, University of Toronto, MSS 3E1 Toronto, Ontario, Canada

Gang Chen – Department of Molecular Genetics, The Donnelly Centre, University of Toronto, MSS 3E1 Toronto, Ontario, Canada

Chao Chen – Department of Molecular Genetics, The Donnelly Centre, University of Toronto, MSS 3E1 Toronto, Ontario, Canada

Alevtina Pavlenco – Department of Molecular Genetics, The Donnelly Centre, University of Toronto, MSS 3E1 Toronto, Ontario, Canada

Reza Saberianfar – Department of Molecular Genetics, The Donnelly Centre, University of Toronto, MSS 3E1 Toronto, Ontario, Canada

Francesca Caccuri – Section of Microbiology, Department of Molecular and Translational Medicine, University of Brescia Medical School, 25123 Brescia, Italy

Alberto Zani – Section of Microbiology, Department of Molecular and Translational Medicine, University of Brescia Medical School, 25123 Brescia, Italy

Nitin Sharma – Department of Pathology and Immunology, Washington University School of Medicine in St Louis, St Louis, Missouri 63110, United States

Annie Feng – Department of Pathology and Immunology, Washington University School of Medicine in St Louis, St Louis, Missouri 63110, United States; Division of Infectious Diseases, John T. Milliken Department of Medicine, Washington University School of Medicine, St. Louis, Missouri 63110, United States

Daisy W. Leung – Division of Infectious Diseases, John T. Milliken Department of Medicine, Washington University School of Medicine, St. Louis, Missouri 63110, United States

Arnaldo Caruso – Section of Microbiology, Department of Molecular and Translational Medicine, University of Brescia Medical School, 25123 Brescia, Italy

Giuseppe Novelli – Department of Biomedicine and Prevention, University of Rome Tor Vergata, 00133 Rome, Italy; Italy 6 IRCCS Neuromed, Pozzilli (IS) 86077, Italy; Department of Pharmacology, School of Medicine, University of Nevada, Reno, Nevada 89557, United States

Gaya K. Amarasinghe – Department of Pathology and Immunology, Washington University School of Medicine in St. Louis, St. Louis, Missouri 63110, United States

Complete contact information is available at:

<https://pubs.acs.org/10.1021/acscchembio.2c00411>

### Author Contributions

<sup>○</sup>J.M.L. and S.M. contributed equally to this work.

### Funding

This study was partially supported by grants from the Canadian Institutes of Health Operating Grant COVID-19 Rapid Research Funding Opportunity OV3-170649, Emergent Ventures/ThistleDown Foundation FAST Grant, Emergent Ventures/The Mercatus Center FAST (#2161 and #2189), and Temerty Foundation Knowledge Translation Grant—Novel Antibody Tools for COVID-19. The infrastructure was supported by a Canada Foundation for Innovation Infrastructure and Operating Grant #IOF-33363, Rome Foundation (Italy, Prot 317A/I) 592, the Italian Ministry of University and Research (FISR2020IP\_03161), and Regione Lazio to G.N.

### Notes

The authors declare the following competing financial interest(s): JML, SM, and SS have filed a patent for CoV-2 binding peptides and uses thereof.

### ACKNOWLEDGMENTS

The authors are grateful to D. Lapa (INMI) for his contribution to determining the neutralizing potency of the antibodies tested in Rome.

### NOMENCLATURE

SARS-CoV-2, severe acute respiratory syndrome coronavirus-2; S-protein, spike protein; RBD, receptor-binding domain; NTD, N-terminal domain; ECD, extracellular domain; VoC, variants of concern; ACE2, angiotensin-converting enzyme 2; R1–R4, RBD-binding peptides 1–4; N1–N4, NTD-binding peptides 1–4; nAbs, neutralizing antibodies; HC, IgG heavy chain; LC, IgG light chain; 33, neutralizing antibody 15033; 33-7, neutralizing antibody 15033-7; NAV, neutravidin

### REFERENCES

- (1) Gazit, S.; Shlezinger, R.; Perez, G.; Lotan, R.; Peretz, A.; Ben-Tov, A.; Cohen, D.; Muhsen, K.; Chodick, G.; Patalon, T. Comparing SARS-CoV-2 natural immunity to vaccine-induced immunity: reinfections versus breakthrough infections. *medRxiv* **2021**.
- (2) Wang, P.; Nair, M. S.; Liu, L.; Iketani, S.; Luo, Y.; Guo, Y.; Wang, M.; Yu, J.; Zhang, B.; Kwong, P. D.; et al. Antibody resistance of SARS-CoV-2 variants B.1.351 and B.1.1.7. *Nature* **2021**, *593*, 130–135.
- (3) Cho, A.; Muecksch, F.; Schaefer-Babajew, D.; Wang, Z.; Finklin, S.; Gaebler, C.; Ramos, V.; Cipolla, M.; Mendoza, P.; Agudelo, M.;

et al. Anti-SARS-CoV-2 receptor binding domain antibody evolution after mRNA vaccination. *Nature* **2021**, *600*, 517–522.

- (4) Arora, P.; Rocha, C.; Kempf, A.; Nehlmeier, I.; Graichen, L.; Winkler, M. S.; Lier, M.; Schulz, S.; Jäck, H.-M.; Cossmann, A.; et al. The spike protein of SARS-CoV-2 variant A.30 is heavily mutated and evades vaccine-induced antibodies with high efficiency. *Cell Mol Immunol* **2021**, *18*, 2673–2675.

- (5) Wrapp, D.; Wang, N.; Corbett, K. S.; Goldsmith, J. A.; Hsieh, C.-L.; Abiona, O.; Graham, B. S.; McLellan, J. S. Cryo-EM structure of the 2019-nCoV spike in the prefusion conformation. *Science* **2020**, *367*, 1260–1263.

- (6) Bosch, B. J.; van der Zee, R.; de Haan, C. A. M.; Rottier, P. J. M. The coronavirus spike protein is a class I virus fusion protein: structural and functional characterization of the fusion core complex. *J. Virol* **2003**, *77*, 8801–8811.

- (7) Yan, R.; Zhang, Y.; Li, Y.; Xia, L.; Guo, Y.; Zhou, Q. Structural basis for the recognition of SARS-CoV-2 by full-length human ACE2. *Science* **2020**, *367*, 1444–1448.

- (8) Jones, B. E.; Brown-Augsburger, P. L.; Corbett, K. S.; Westendorf, K.; Davies, J.; Cujec, T. P.; Wiethoff, C. M.; Blackbourne, J. L.; Heinz, B. A.; et al. The neutralizing antibody, LY-CoV555, protects against SARS-CoV-2 infection in nonhuman primates. *Sci. Transl. Med.* **2021**, *13*, eabf1906.

- (9) Liu, L.; Wang, P.; Nair, M. S.; Yu, J.; Rapp, M.; Wang, Q.; Luo, Y.; Chan, J. F.-W.; Sahi, V.; Figueroa, A.; et al. Potent neutralizing antibodies against multiple epitopes on SARS-CoV-2 spike. *Nature* **2020**, *584*, 450–456.

- (10) Hansen, J.; Baum, A.; Pascal, K. E.; Russo, V.; Giordano, S.; Wloga, E.; Fulton, B. O.; Yan, Y.; Koon, K.; Patel, K.; et al. Studies in humanized mice and convalescent humans yield a SARS-CoV-2 antibody cocktail. *Science* **2020**, *369*, 1010–1014.

- (11) Zhou, D.; Duyvesteyn, H. M. E.; Chen, C.-P.; Huang, C.-G.; Chen, T.-H.; Shih, S.-R.; Lin, Y.-C.; Cheng, C.-Y.; Cheng, S.-H.; Huang, Y.-C.; et al. Structural basis for the neutralization of SARS-CoV-2 by an antibody from a convalescent patient. *Nat Struct Mol Biol* **2020**, *27*, 950–958.

- (12) Du, S.; Cao, Y.; Zhu, Q.; Yu, P.; Qi, F.; Wang, G.; Du, X.; Bao, L.; Deng, W.; Zhu, H.; et al. Structurally Resolved SARS-CoV-2 Antibody Shows High Efficacy in Severely Infected Hamsters and Provides a Potent Cocktail Pairing Strategy. *Cell* **2020**, *183*, 1013–1023.e13.

- (13) Ju, B.; Zhang, Q.; Ge, J.; Wang, R.; Sun, J.; Ge, X.; Yu, J.; Shan, S.; Zhou, B.; Song, S.; et al. Human neutralizing antibodies elicited by SARS-CoV-2 infection. *Nature* **2020**, *584*, 115–119.

- (14) Wu, Y.; Wang, F.; Shen, C.; Peng, W.; Li, D.; Zhao, C.; Li, Z.; Li, S.; Bi, Y.; Yang, Y.; et al. A noncompeting pair of human neutralizing antibodies block COVID-19 virus binding to its receptor ACE2. *Science* **2020**, *368*, 1274–1278.

- (15) Taylor, P. C.; Adams, A. C.; Hufford, M. M.; de la Torre, I.; Winthrop, K.; Gottlieb, R. L. Neutralizing monoclonal antibodies for treatment of COVID-19. *Nat. Rev. Immunol.* **2021**, *21*, 382–393.

- (16) Zhu, X.; Mannar, D.; Srivastava, S. S.; Berezuk, A. M.; Demers, J.-P.; Saville, J. W.; Leopold, K.; Li, W.; Dimitrov, D. S.; Tuttle, et al. Cryo-electron microscopy structures of the N501Y SARS-CoV-2 spike protein in complex with ACE2 and 2 potent neutralizing antibodies. *PLoS Biol.* **2021**, *19*, No. e3001237.

- (17) De Gasparo, R.; Pedotti, M.; Simonelli, L.; Nickl, P.; Muecksch, F.; Cassaniti, I.; Percivalle, E.; Lorenzi, J. C. C.; Mazzola, F.; Magri, D.; et al. Bispecific IgG neutralizes SARS-CoV-2 variants and prevents escape in mice. *Nature* **2021**, *593*, 424–428.

- (18) Rujas, E.; Kucharska, I.; Tan, Y. Z.; Benlekbir, S.; Cui, H.; Zhao, T.; Wasney, G. A.; Budyłowski, P.; Guvenç, F.; Newton, J. C.; et al. Multivalency transforms SARS-CoV-2 antibodies into ultra-potent neutralizers. *Nat. Commun.* **2021**, *12*, No. 3661.

- (19) Cao, L.; Goresnik, I.; Coventry, B.; Case, J. B.; Miller, L.; Kozodoy, L.; Chen, R. E.; Carter, L.; Walls, A. C.; Park, Y.-J.; et al. De novo design of picomolar SARS-CoV-2 miniprotein inhibitors. *Science* **2020**, *370*, 426–431.

- (20) Miersch, S.; Li, Z.; Saberianfar, R.; Ustav, M.; Brett Case, J.; Blazer, L.; Chen, C.; Ye, W.; Pavlenco, A.; Gorelik, M.; et al. Tetravalent SARS-CoV-2 Neutralizing Antibodies Show Enhanced Potency and Resistance to Escape Mutations. *J. Mol. Biol.* **2021**, *433*, No. 167177.
- (21) Pomplun, S.; Jbara, M.; Quartararo, A. J.; Zhang, G.; Brown, J. S.; Lee, Y.-C.; Ye, X.; Hanna, S.; Pentelute, B. L. De Novo Discovery of High-Affinity Peptide Binders for the SARS-CoV-2 Spike Protein. *ACS Cent. Sci.* **2021**, *7*, 156–163.
- (22) Arita, Y.; Allen, S.; Chen, G.; Zhang, W.; Wang, Y.; Owen, A. J.; Dentinger, P.; Sidhu, S. S. Rapid isolation of peptidic inhibitors of the solute carrier family transporters OATP1B1 and OATP1B3 by cell-based phage display selections. *Biochem. Biophys. Res. Commun.* **2016**, *473*, 370–376.
- (23) Bozovičar, K.; Bratkovič, T. Small and Simple, yet Sturdy: Conformationally Constrained Peptides with Remarkable Properties. *Int. J. Mol. Sci.* **2021**, *22*, 1611.
- (24) Jain, T.; Sun, T.; Durand, S.; Hall, A.; Houston, N. R.; Nett, J. H.; Sharkey, B.; Bobrowicz, B.; Caffry, I.; Yu, Y.; et al. Biophysical properties of the clinical-stage antibody landscape. *Proc. Natl. Acad. Sci. U.S.A.* **2017**, *114*, 944–949.
- (25) Chen, R.; Le Rouzic, E.; Kearney, J. A.; Mansky, L. M.; Benichou, S. Vpr-mediated incorporation of UNG2 into HIV-1 particles is required to modulate the virus mutation rate and for replication in macrophages. *J. Biol. Chem.* **2004**, *279*, 28419–28425.
- (26) Yan, R.; Wang, R.; Ju, B.; Yu, J.; Zhang, Y.; Liu, N.; Wang, J.; Zhang, Q.; Chen, P.; Zhou, B.; et al. Structural basis for bivalent binding and inhibition of SARS-CoV-2 infection by human potent neutralizing antibodies. *Cell Res.* **2021**, *31*, 517–525.
- (27) Autio, K. A.; Boni, V.; Humphrey, R. W.; Naing, A. Probody Therapeutics: An Emerging Class of Therapies Designed to Enhance On-Target Effects with Reduced Off-Tumor Toxicity for Use in Immuno-Oncology. *Clin. Cancer Res.* **2020**, *26*, 984–989.
- (28) Polu, K. R.; Lowman, H. B. Probody therapeutics for targeting antibodies to diseased tissue. *Expert Opin. Biol. Ther.* **2014**, *14*, 1049–1053.
- (29) Stroh, M.; Sagert, J.; Burke, J. M.; Apgar, J. F.; Lin, L.; Millard, B. L.; Michael Kavanaugh, W. Quantitative Systems Pharmacology Model of a Masked, Tumor-Activated Antibody. *CPT Pharmacometrics Syst. Pharmacol.* **2019**, *8*, 676–684.
- (30) Desnoyers, L. R.; Vasiljeva, O.; Richardson, J. H.; Yang, A.; Menendez, E. E. M.; Liang, T. W.; Wong, C.; Bessette, P. H.; Kamath, K.; Moore.; et al. Tumor-specific activation of an EGFR-targeting probody enhances therapeutic index. *Sci. Transl. Med.* **2013**, *5*, 207ra144.
- (31) Sanborn, R. E.; Hamid, O.; de Vries, E. G.; Ott, P. A.; Garcia-Corbacho, J.; Boni, V.; Bendell, J.; Autio, K. A.; Cho, D. C.; Plummer, R.; et al. CX-072 (pacmilimab), a Probody PD-L1 inhibitor, in combination with ipilimumab in patients with advanced solid tumors (PROCLAIM-CX-072): a first-in-human, dose-finding study. *J. Immunother. Cancer* **2021**, *9*, No. e002446.
- (32) Tonikian, R.; Zhang, Y.; Boone, C.; Sidhu, S. S. Identifying specificity profiles for peptide recognition modules from phage-displayed peptide libraries. *Nat. Protoc.* **2007**, *2*, 1368–1386.
- (33) Case, J. B.; Rothlauf, P. W.; Chen, R. E.; Liu, Z.; Zhao, H.; Kim, A. S.; Bloyet, L.-M.; Zeng, Q.; Tahan, S.; Droit, L.; et al. Neutralizing Antibody and Soluble ACE2 Inhibition of a Replication-Competent VSV-SARS-CoV-2 and a Clinical Isolate of SARS-CoV-2. *Cell Host Microbe* **2020**, *28*, 475–485.e5.
- (34) Case, J. B.; Rothlauf, P. W.; Chen, R. E.; Kafai, N. M.; Fox, J. M.; Smith, B. K.; Shrihari, S.; McCune, B. T.; Harvey, I. B.; Keeler, S. P.; et al. Replication-Competent Vesicular Stomatitis Virus Vaccine Vector Protects against SARS-CoV-2-Mediated Pathogenesis in Mice. *Cell Host Microbe* **2020**, *28*, 465–474.e4.
- (35) Caccuri, F.; Zani, A.; Messali, S.; Giovanetti, M.; Bugatti, A.; Campisi, G.; Filippini, F.; Scaltriti, E.; Ciccozzi, M.; Fiorentini, S.; Caruso, A. A persistently replicating SARS-CoV-2 variant derived from an asymptomatic individual. *J. Transl. Med.* **2020**, *18*, 362.
- (36) VanBlargan, L. A.; Errico, J. M.; Halfmann, P. J.; Zost, S. J.; Crowe, J. E.; Purcell, L. A.; Kawaoka, Y.; Corti, D.; Fremont, D. H.; Diamond, M. S. An infectious SARS-CoV-2 B.1.1.529 Omicron virus escapes neutralization by therapeutic monoclonal antibodies. *Nat. Med.* **2022**, *28*, 490–495.
- (37) Manenti, A.; Maggetti, M.; Casa, E.; Martinuzzi, D.; Torelli, A.; Trombetta, C. M.; Marchi, S.; Montomoli, E. Evaluation of SARS-CoV-2 neutralizing antibodies using a CPE-based colorimetric live virus micro-neutralization assay in human serum samples. *J. Med. Virol.* **2020**, *92*, 2096–2104.